Pharm Res (2013) 30:552–561
DOI 10.1007/s11095-012-0900-8

RESEARCH PAPER

Block Copolymer Cross-Linked Nanoassemblies Improve Particle Stability and Biocompatibility of Superparamagnetic Iron Oxide Nanoparticles

Mo Dan • Daniel F. Scott • Peter A. Hardy • Robert J. Wydra • J. Zach Hilt • Robert A. Yokel • Younsoo Bae

Received: 7 August 2012 / Accepted: 8 October 2012 / Published online: 19 October 2012

ABSTRACT

Purpose To develop cross-linked nanoassemblies (CNAs) as carriers for superparamagnetic iron oxide nanoparticles (IONPs).

Methods Ferric and ferrous ions were co-precipitated inside core-shell type nanoparticles prepared by cross-linking poly (ethylene glycol)-poly(aspartate) block copolymers to prepare CNAs entrapping Fe_3O_4 IONPs (CNA-IONPs). Particle stability and biocompatibility of CNA-IONPs were characterized in comparison to citrate-coated Fe_3O_4 IONPs (Citrate-IONPs).

Results CNA-IONPs, approximately 30 nm in diameter, showed no precipitation in water, PBS, or a cell culture medium after 3 or 30 h, at 22, 37, and 43°C, and 1, 2.5, and 5 mg/mL, whereas Citrate-IONPs agglomerated rapidly (> 400 nm) in all aqueous media tested. No cytotoxicity was observed in a mouse brain endothelial-derived cell line (bEnd.3) exposed to CNA-IONPs up to 10 mg/mL for 30 h. Citrate-IONPs (> 0.05 mg/mL) reduced cell viability after 3 h. CNA-IONPs retained the superparamagnetic properties of entrapped IONPs, enhancing T2-weighted magnetic resonance images (MRI) at 0.02 mg/mL, and generating heat at a mild hyperthermic level (40 ~ 42°C) with an alternating magnetic field (AMF).

Conclusion Compared to citric acid coating, CNAs with a cross-linked anionic core improved particle stability and biocompatibility of IONPs, which would be beneficial for future MRI and AMF-induced remote hyperthermia applications.

KEY WORDS cross-linked nanoassemblies · hyperthermia · magnetic resonance imaging · nanoparticles · superparamagnetic iron oxide

INTRODUCTION

Iron oxide nanoparticles (IONPs) are superparamagnetic materials, which can be activated only in the presence of an external magnetic field, enabling various bionanomedical applications (1,2). For example, IONPs have been used as contrast agents that can enhance T2-weighted (signal darkening) magnetic resonance images (MRI) of tissues *in vivo* (3–5). The particle sizes of IONPs can be tailored to accumulate in specific organs, contributing to early detection of human malignancies with blood vessel disruption (6–8).

IONPs have drawn increasing attention as MRI contrast agents to evaluate blood–brain barrier dysfunction related to tumors and other pathologies in the central nervous system (*e.g.* brain tumor, stroke, and carotid atherosclerosis) in clinical and preclinical studies (9,10). IONPs can be also used as a heating source for hyperthermia as they generate heat in the presence of an alternating magnetic field (AMF) to increase temperature in solutions or localized tissues, thereby killing cancer cells in a controlled manner (11–13). Hyperthermia above 40°C can induce tumor cell death,

M. Dan • D. F. Scott • R. A. Yokel • Y. Bae
Department of Pharmaceutical Sciences
College of Pharmacy, University of Kentucky
Lexington, Kentucky 40536, USA

M. Dan • R. A. Yokel
Graduate Center for Toxicology, University of Kentucky
Lexington, Kentucky 40536, USA

P. A. Hardy
Anatomy and Neurobiology, University of Kentucky
Lexington, Kentucky 40536, USA

R. J. Wydra • J. Z. Hilt
Chemical and Materials Engineering, University of Kentucky
Lexington, Kentucky 40506, USA

Y. Bae (✉)
Department of Pharmaceutical Sciences, College of Pharmacy
University of Kentucky
789 South Limestone
Lexington, Kentucky 40536-0596, USA
e-mail: younsoo.bae@uky.edu

because tumor cells are susceptible to sudden temperature increases (14). One major problem for conventional hyperthermia therapy is to increase temperature to a therapeutic level in the center of the tumor (7). A clinical study showed that hyperthermia using IONPs in conjunction with a reduced radiation dose led to longer survival of patients compared to conventional therapies in the treatment of recurrent glioblastoma (15). This dual functionality (*i.e.* T2 MRI enhancement and AMF-induced remote heating) makes IONPs useful for novel applications combining both diagnosis and therapy of human diseases, an application often referred to as theranostics (16,17). Theranostics is important particularly for the treatment of tumors in delicate organs, susceptible to drugs, heat, or other physicochemical stress factors (*e.g.* the brain).

A problem with IONPs is their tendency to agglomerate in aqueous solutions unless their surface is properly modified, resulting in plasma protein binding *in vivo* and rapid clearance by the mononuclear phagocyte system (MPS) (18). Aggregation of IONPs leads to altered magnetic properties or even complete loss of magnetism (19). In addition, IONPs are easily oxidized, transforming from magnetite (Fe_3O_4) to maghemite (γFe_2O_3), leading to a broad spectrum of particle size, shape, stability, and magnetic properties (20,21). Several studies showed that IONPs, either bare or surface-modified, could cause cell toxicity and oxidative stress *in vitro* and *in vivo* (22–24). Therefore, it is crucial to improve particle stability and biocompatibility of IONPs in biological environment. Numerous efforts have been made to suppress agglomeration and retain the superparamagnetic properties of IONPs for a prolonged time (25–27). Citric acid and surfactants are frequently used to stabilize IONPs in aqueous solutions (28–30), but these stabilizers often cause problems. For example, although citric acid forms a stable chelate with Fe_3O_4 iron oxide, it is not sufficient to prevent agglomeration and precipitation in the presence of multivalent counter ions (magnesium or calcium) and serum proteins (31–34). Surfactants, typically prepared from multivalent polymers, have been also developed to stabilize IONPs *in vivo*, yet they can get detached from IONPs due to an unclear mechanism by which ligand exchange occurs in metal chelates (35–37). Importantly, these IONP formulations, which change particle stability over time *in vivo*, could potentially cause toxic effects *in vivo* (38,39).

Biocompatible polymer nanoparticles and water soluble polymers have been used as less toxic and more stable alternatives to these stabilizers (19,20). Among these polymer-based formulations, polymeric micelles from amphiphilic block copolymers are an attractive choice to develop IONP formulations for cancer imaging and hyperthermia (40,41). Micelles can embed IONPs and achieve considerable MRI contrast enhancement as a result of the collective effects of IONP clusters (42–44). However, one of the critical problems associated with conventional polymeric micelles is particle stability, particularly in dilute conditions (*e.g.* blood and other biological environments) as polymer micelles can dissociate below the critical micelle concentration (45). To solve these problems, we recently developed cross-linked nanoassemblies (CNAs) from biocompatible poly(ethylene glycol)-poly(aspartate) [PEG-p(Asp)] block copolymers, which provided stable nanoparticles that can entrap charged, hydrophobic, and amphiphilic payloads without changing particle sizes optimized for tumor accumulation (< 100 nm) (46–48). We hypothesized that CNAs containing carboxyl groups in the core would simultaneously create, entrap, and protect IONPs as iron ions (Fe^{2+} and Fe^{3+}) co-precipitate inside the nanoassembly core, thus suppressing IONP agglomeration (Fig. 1). In this study, we tested our hypothesis and confirmed that IONPs incorporated into CNAs improve their particle stability and biocompatibility in aqueous solutions without compromising paramagnetic properties.

Particle stability and biocompatibility were determined with or without 30 min AMF exposure in water, phosphate buffered saline (PBS), and a cell culture medium with 10% fetal bovine serum (FBS) at 22, 37, and 43°C, corresponding to room, body, and hyperthermic temperatures, respectively. Cytotoxicity of the particles was investigated using a

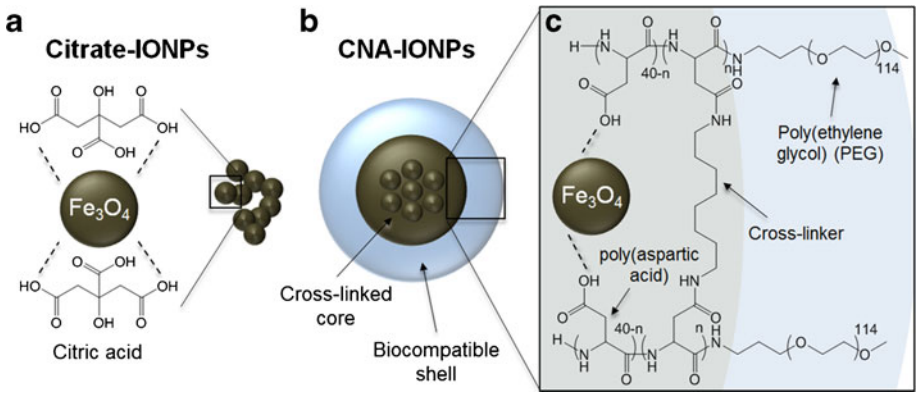

Fig. 1 Citrate-coated iron oxide nanoparticles (Citrate-IONPs) and cross-linked nanoassemblies entrapping IONPs (CNA-IONPs). (**a**) A chelate is formed between citric acid and Fe_3O_4 iron oxide; (**b**) CNA-IONPs entrap Fe_3O_4 in the core to protect the iron oxide from agglomeration and protein binding; and (**c**) Fe_3O_4 IONPs are stabilized in the cross-linked core of CNAs.

mouse brain endothelial-derived cell line (bEnd.3). To evaluate potential imaging applications, T2-weighted MRI enhancement of CNA-IONPs was tested in water, PBS and a cell culture medium. AMF-induced heating properties of 1, 2.5 and 5 mg/mL CNA-IONPs were also evaluated in a cell culture medium for future hyperthermia applications. Conventional citrate-coated IONPs (Citrate-IONPs) were used as control. Results of this study provide insight into potential applications of CNA-IONPs, integrating MRI diagnosis and thermal therapy.

MATERIALS AND METHODS

Materials

N,N′-Diisopropylcarbodiimide (DIC), N-hydroxysuccinimide (NHS), 4-(dimethylamino)pyridine (DMAP), β-benzyl L-aspartate, triphosgene, hexane, benzene, tetrahydrofuran (THF), dimethyl sulfoxide (DMSO), ferrous chloride tetrahydrate ($FeCl_2 \cdot 4H_2O$), ferric chloride hexahydrate ($FeCl_3 \cdot 6H_2O$), ammonium hydroxide (NH_4OH), citric acid monohydrate, and ethanol (100%) were purchased from Sigma-Aldrich (St. Louis, MO, USA). α-Methoxy-ω-amino poly(ethylene glycol) (PEG, 5 kDa) was purchased from the NOF Corporation (Tokyo, Japan). Cell culture medium Dulbecco's Modified Eagle Medium (DMEM), regenerated cellulose dialysis bags with 6 ~ 8 kDa molecular weight cut off (MWCO), sodium hydroxide (NaOH), and hydrochloric acid (HCl) were purchased from Fisher Scientific (USA). FBS was purchased from Atlanta Biologicals (Lawrenceville, GA, USA) and penicillin-streptomycin (Pen-Strep) was purchased from Invitrogen (Grand Island, NY, USA).

Synthesis of CNAs

CNAs were prepared by cross-linking poly(ethylene glycol)-poly(aspartate) [PEG-p(Asp)] block copolymers as previously reported with slight modification (46). Briefly, β-Benzyl-L-aspartate N-carboxy anhydride (BLA-NCA) monomers were prepared by reacting β-benzyl-L-aspartate with triphosgene (1.3 equivalent) in dry THF at 45°C until the solution became clear. Anhydrous hexane was added to the BLA-NCA, which was subsequently recrystallized at −20°C. As shown in Fig. 2, BLA-NCA monomers were polymerized using amino-terminated 5 kDa PEG as a macroinitiator in DMSO (50 mg/mL) at 45°C under dry nitrogen for 48 h to synthesize PEG-poly(β-benzyl L-aspartate) (PEG-PBLA). PEG-PBLA was collected from the reaction solution by precipitation in diethyl ether and freeze drying from benzene. ^{1}H-NMR (400 MHz, Varian) spectra from PEG (3.5 ppm) and benzyl groups (7.3 ppm) was used to determine the block copolymer composition. PEG-PBLA with 40 aspartate repeating units was used for this study. The benzyl groups of PEG-PBLA were removed by 0.1 N NaOH. The benzyl alcohol byproducts and excess NaOH were removed through dialysis, followed by desalination of the aspartate through the addition of HCl to the dialysis solution to yield PEG-p(Asp). To prepare CNAs, PEG-p(Asp) was dissolved in DMSO to a final concentration of 75 mg/mL followed by the addition of DIC, NHS, and DMAP (in a molar ratio of 4:4:0.2, respectively) to the aspartate units of PEG-p(Asp). A 0.5 molar equivalent of 1,8-diaminooctane was added to the reaction solution, which was placed at 50°C for 72 h. The CNAs were dialyzed against 100% DMSO, 50% DMSO, and finally deionized water to remove impurities, followed by freeze

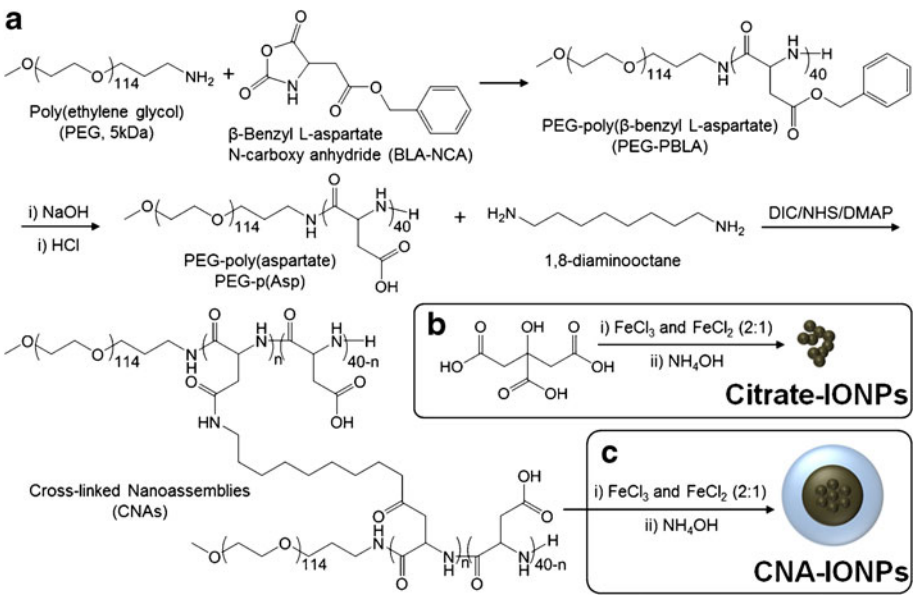

Fig. 2 Synthesis schemes for empty CNAs (**a**), citrate-IONPs (**b**), and CNA-IONPs (**c**).

drying. CNA purity was characterized with gel permeation chromatography (GPC, Shimadzu LC20, Japan), which was equipped with refractive index (RI) and ultraviolet (UV) detectors. PEG standards were used to establish a calibration curve for molecular weight determination (Mn = number molecular weight).

Preparation of Citrate-IONPs and CNA-IONPs

Citrate-IONPs were prepared by co-precipitating iron oxides and citric acid in an aqueous solution as previously reported (2). As shown in Fig. 2b, ferric chloride hexahydrate (Fe^{3+}) and ferrous chloride tetrahydrate (Fe^{2+}) were dissolved in deionized water (Fe^{3+} Fe^{2+}=2:1), followed by adding ammonium hydroxide dropwise under an N_2 atmosphere at 85°C. Citric acid (2 equivalent) was then added to prepare Citrate-IONPs. After 1 h, the solution was placed on a magnet to collect black brown particles, which were washed repeatedly using pure ethanol (28,49). Citrate-IONPs were dried overnight in a vacuum drying oven.

CNA-IONPs were prepared similarly by mixing ferric and ferrous salts at a 2:1 molar ratio with CNAs in deionized water (Fig. 2c). The total iron ions and the carboxyl groups of CNAs were adjusted in a molar ratio of 1:2. Ammonium hydroxide was added to this mixed solution dropwise under nitrogen atmosphere and the reaction was allowed to proceed at 85°C for 1 h. The solution was centrifuged at 3,000 g for 5 min to remove precipitates and other water-insoluble impurities. CNA-IONPs in the supernatant were dialyzed (MWCO 6~8 kDa), filtered (0.22 μm syringe filters), and collected by freeze drying.

Particle Characterization

The particle size distribution was determined by dynamic light scattering (DLS) analysis (90Plus NanoParticle size distribution analyzer, Brookhaven Instruments, Holtsville, NY, USA). Zeta potential was measured with Zetasizer Nano ZS (Malvern Instruments, Worcestershire, UK). The IONP loading content for CNA-IONPs was quantified by thermal gravimetric analysis (TGA, Perkin-Elmer TGA7 Analyzer, Waltham, MA, USA) and inductively coupled plasma mass spectrometry (ICP-MS, Agilent 7500cx, Santa Clara, CA, USA). TGA and ICP-MS determined the amount of iron remaining from CNA-IONPs, following thermal decomposition (100~600°C) and chemical digestion (HNO_3:H_2O_2=2:1) of CNAs, respectively.

Particle Size and Stability Evaluation in Aqueous Media

Particle size and stability of Citrate-IONPs and CNA-IONPs (0.1 mg/mL, based on IONP content) were first observed by dissolving the particles in water, PBS, and DMEM with 10% FBS and 1% Pen-Strep, using 1.5 mL microvials. Aqueous solubility, particle size, and stability of Citrate-IONPs and CNA-IONPs were further characterized under various media: in water at 1 mg/mL, 22°C, for 30 h; in water at 1 mg/mL, 37°C, for 30 h; in cell culture medium at 1 mg/mL, 37°C, for 30 h; and in cell culture medium at 1 mg/mL, 43°C, for 30 h, as discussed in detail in the "Results and Discussion" section. DLS was used to monitor time-dependent changes in particle size of all samples.

Cytotoxicity Assays

A mouse brain endothelial cell line (bEnd.3) was obtained from American Type Culture Collection (CRL-2299). The cells were cultured in a humidified incubator (37°C and 5% CO_2) and used from passages 5 through 10. Cells were seeded on 96 well plates (4,000 cells/well) and incubated with DMEM supplemented with 10% FBS and 1% Pen-Strep for 24 h. These cells were treated with Citrate-IONPs (0, 0.002, 0.02, 0.05, 0.1, and 0.2 mg/mL) and CNA-IONPs (0, 0.2, 0.5, 1, 5, and 10 mg/mL). Citrate-IONP and CNA-IONP concentrations were based on cytotoxicity observed in preliminary experiments. The cells were incubated with Citrate-IONPs or CNA-IONPs for 0.5, 3, 6, 12 and 30 h, followed by washing the cells with PBS three times. After additional 24 h incubation in fresh cell culture media, cell viability was determined using the resazurin dye assay. Resazurin in PBS was added to the cell-containing wells to a final concentration of 100 μM. Cell plates were incubated for an additional 3 h as non-fluorescent resazurin was converted to fluorescent resorufin by live cells (50,51). Resorufin signals were measured at λ_{ex} 485 nm and λ_{em}530 nm. Cell viability was reported as % of control at the same time.

Magnetic Resonance Imaging

Citrate-IONPs and CNA-IONPs were dispersed in water, PBS, and cell culture media with two-fold serial dilutions ranging from 0.02 to 2.5 mg/mL (based on IONP content). Citrate-IONP and CNA-IONP solutions (150 μL) were placed in a 96 well plate and imaged on a 3.0 Tesla MR imager (Siemens Tim Trio, Erlangen, Germany) using a 10 cm diameter surface coil to enhance the received signal. Multiple, T2-weighted fast spin echo images of all samples were acquired with different echo time (TE), to visualize the dependence of the T2 relaxation time on the particle composition and dispersing media. From the multi echo T2 images acquired at different echo times, we used a custom-developed software code to derive T2 on a pixel-by-pixel basis. From these images we estimated the average T2

within the wells of CNA-IONPs in the three media as a function of particle concentration.

Evaluation of AMF-Induced Heating Profiles and Particle Stability After AMF Exposure

The heating profiles of CNA-IONPs were evaluated in cell culture media (1, 2.5, and 5 mg/mL) under AMF induced by a Taylor Winfield induction power supply (Taylor-Winfield Technologies MMF-3-135/400-2, Columbus, OH, USA) equipped with a 15 mm diameter, 5 turn solenoid. The AMF field parameters were set to 59.3 kA/m at 300 kHz for 30 min. The temperature of the medium was measured every 0.25 s for 30 min using a Fluoroptic® thermometer (LumaSense Technologies, Santa Clara, CA, USA). The initial medium temperature was 37°C. The CNA-IONP particle stability was monitored in cell culture media (1, 2.5, and 5 mg/mL) for 30 h after 30 min AMF using DLS.

Statistical Analysis

One-way ANOVA followed by Tukey's test was used to test for significant differences among particle sizes of the samples with different incubation times and temperatures. Two-way ANOVA followed by Bonferroni multiple comparisons was used to test for significant differences among different concentration groups and times (GraphPad Prism Version 3.00 for Windows, GraphPad Software, San Diego, CA). Statistical significance was accepted at a level of $p<0.05$. All results are reported as mean ± standard deviation (SD).

RESULTS AND DISCUSSION

Preparation and Characterization of Citrate-IONPs and CNA-IONPs

GPC analyses confirmed that CNAs were successfully formed with narrow dispersity (Fig. 3). Molecular weight of CNAs was 304,007 Da, indicating that approximately 32 PEG-p(Asp) block copolymer chains formed an individual CNA particle. No free PEG-p(Asp) block copolymers (Mn=9,600 Da) were seen after CNA synthesis, although small molecular weight impurities (Mn=2,859 Da) were observed. The particle size of empty CNAs was 36±5 nm. These results were consistent with our previous observations for other CNAs (46,47). The solution containing IONPs formed dark brown precipitates immediately after NH_4OH was added in the presence of either citric acid or empty CNAs. In comparison to Citrate-IONPs, CNA-IONPs remained soluble in aqueous solutions even after centrifugation. As a result, unreacted iron ions, aggregated

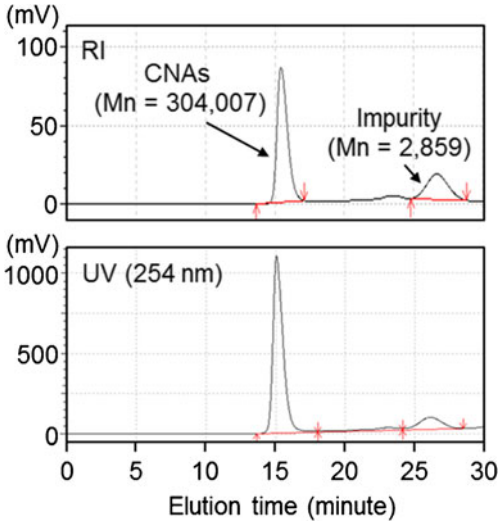

Fig. 3 Gel permeation chromatography (GPC) spectra of CNAs.

IONPs, and other impurities were readily removed from CNA-IONPs. Subsequent DLS measurements showed that CNA-IONPs were 25±3 nm, similar to empty CNAs, indicating that the cross-linked core of CNAs effectively suppressed the growth of IONPs inside the nanoassemblies, preventing aggregation. Citrate-IONPs were initially 90± 10 nm in water at 200 μg/mL, but their particle sizes varied as agglomeration and precipitation occurred (discussed in detail in the "Particle Stability" section). CNA-IONPs showed 25±3 and 25±1% (wt%) IONP loading, determined by TGA and ICP-MS analyses, respectively. Zeta potentials of Citrate-IONPs and CNA-IONPs in PBS at pH 7.4 were −29.5±3.6 and −5.0±0.6 mV, respectively. These results suggested that CNA-IONPs effectively protected IONPs inside the carboxyl-rich nanoassembly core, shielding the electric charge of IONP chelates with CNAs.

Particle Stability

Citrate-IONPs and CNA-IONPs were first dispersed in water, PBS, and cell culture media at 0.1 mg/mL for solubility testing (Fig. 4). Citrate-IONPs dispersed partially in aqueous solutions, but the solutions were turbid (Fig. 4a), forming precipitates (Fig. 4b, blue box). On the other hand, CNA-IONPs were stable in all aqueous solutions: the letters 'IO' can be seen clearly through the brown solution in Fig. 4a and no precipitates are seen in Fig. 4b (red box). Interestingly, Citrate-IONPs remained at around 400 nm in the serum-containing cell culture medium at 37°C for 3 h, but they ultimately precipitated in water, PBS, and DMEM (Fig. 5a). It is surmised that Citrate-IONPs in the cell culture medium might have bound to bovine serum albumin (BSA) from 10% FBS, forming 400 nm complexes that dispersed in the solution as previous studies reported that BSA

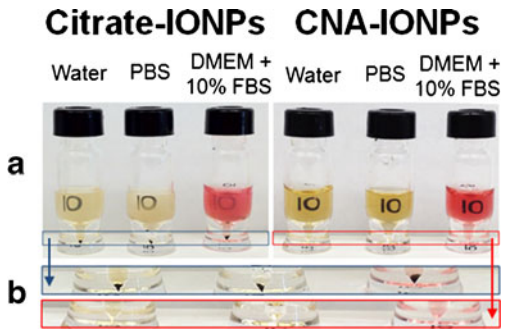

Fig. 4 Citrate-IONPs and CNA-IONPs in aqueous solutions. (**a**) Turbidity of sample solutions at 0.1 mg/mL; and (**b**) Enlarged images of the bottom of a 1.5 mL glass vial showing precipitates of Citrate-IONPs [blue box] but not CNA-IONPs [red box].

stabilized metal oxide nanoparticles (52–54). Nevertheless, rapid agglomeration in the cell culture medium to > 400 nm will still likely limit biomedical applications of Citrate-IONPs. Previous research demonstrated that IONPs smaller than 50 nm had a longer circulation time in blood than larger IONPs that were rapidly cleared by the MPS (55).

CNA-IONPs were stable in water and cell culture media at 22, 37, and 43°C for 30 h, and particle size remained unchanged between 25 ~ 29 nm in diameter (Figs. 5a and b). There were no significant changes in the particle size of CNA-IONP from 1 to 5 mg/ml (Fig. 5c). A previous study showed that the magnetic property of IONPs is size-dependent and that the particle size is linearly correlated with the saturation magnetization of IONPs (56). As mentioned above, IONPs below 50 nm can circumvent the MPS and have a longer circulation time (55). Several researchers demonstrated plasma proteins rapidly bound to nanoparticle surfaces, forming a protein corona which can change nanomaterial physicochemical properties and influence their fate *in vivo* (57–59). In this study, the presence of 10% FBS in cell culture medium produced no significant change in the particle size of CNA-IONPs over 30 h in a biologically-relevant medium compared with their size in water. In general, the small particle size that remained constant for > 30 h is favorable for *in vivo* applications using CNA-IONPs because particle size-induced changes in IONPs magnetic properties and biodistribution will be minimal. Therefore, these results suggested that CNA-IONPs would be stable in blood *in vivo*, which will be beneficial especially for increasing their blood retention time, and thus potentially improving blood-tumor barrier penetration for diagnosis and therapy of tumors located away from the body surface such as brain (60).

Cytotoxicity of Citrate-IONPs and CNA-IONPs

Time-dependent cytotoxicity of Citrate-IONPs and CNA-IONPs was tested in a murine brain endothelial cell line (bEnd.3) as shown in Fig. 6. Citrate-IONPs caused a significant decrease in cell viability at concentrations greater than 0.05 mg/mL, and cell viability dropped rapidly at 0.1 mg/mL after 3 h (Fig. 6a). This is consistent with previous reports showing IONPs caused serious cytotoxicity in cells, limiting their applications as imaging contrast agents (23), and significantly increased reactive oxygen species (> 0.025 mg/mL) (61). Even FDA-approved MRI contrast agents, such as Endorem® and Sinerem® (derivatized dextran coated IONPs), are reported to cause cell growth inhibition over a 24 h period at 0.05 mg/mL (62), similar to the Citrate-IONPs cytotoxic concentration in this study. Previous studies showed that IONP toxicity *in vitro* was highly dependent on size, surface modification, charge, and cell type (63). However, most IONPs started to show toxicity above 1 mg/mL *in vitro* despite their size, surface modification, charge, or the cell type (23). On the contrary, CNA-IONPs caused no cell death up to 10 mg/mL and 30 h exposure (Fig. 6b). These results demonstrate that CNA-IONPs significantly improved biocompatibility of

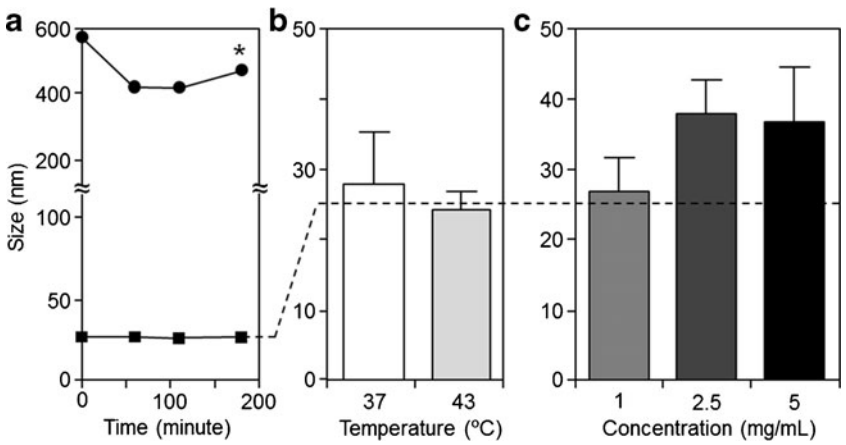

Fig. 5 Particle stability characterization results. Samples were incubated in DMEM cell culture media with 10% FBS. (**a**) Time-dependent changes of particle sizes for Citrate-IONPs [circles] and CNA-IONPs [squares] incubated at room temperature. The asterisk (*) indicates that Citrate-IONPs started precipitating; (**b**) temperature effects on particle sizes for CNA-IONPs incubated for 30 h; and (**c**) concentration effects on particle sizes of CNA-IONPs following 30 min AMF.

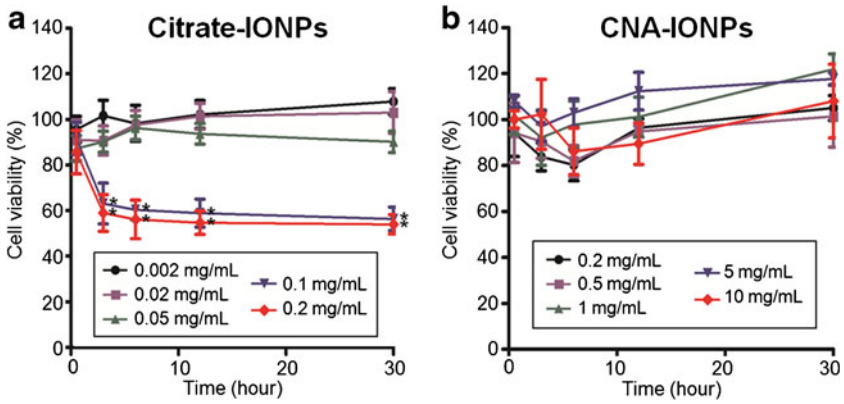

Fig. 6 Biocompatibility characterization results. A mouse brain endothelial cell line (bEnd.3) was incubated with either Citrate-IONPs (**a**) or CNA-IONPs (**b**) at different concentrations and times. The asterisks (*) indicate significant differences ($p < 0.05$) from the three lower concentrations (0.002, 0.02, and 0.05 mg/mL).

IONPs entrapped inside the nanoassemblies as opposed to citrate-IONP formulations.

MRI of Citrate-IONPs and CNA-IONPs

Citrate-IONPs and CNA-IONPs showed concentration-dependent changes on T2-weighted MR images (image darkening) (Fig. 7). Citrate-IONPs showed contrast patterns similar to CNA-IONPs in water, but Citrate-IONPs dispersed initially yet agglomerated gradually in PBS and cell culture media, forming agglomerates on the bottom of wells when placed in the magnetic field of the MR imager. Images acquired transverse to the wells showed that Citrate-IONPs precipitated at the bottom of wells producing zones of intense signal loss on T2 images (side-view images in Fig. 7). Citrate-IONPs showed a dark signal on the T2 images above 0.16 mg/mL in water. Citrate-IONPs were observed to agglomerate faster in cell culture medium than PBS at the same concentration (data not shown), and showed dark images above 0.63 mg/mL.

On the contrary, CNA-IONPs were stable in water, PBS and cell culture media (Fig. 4b, red box), showing concentration-dependent T2-weighted MRI contrast (Fig. 7). CNA-IONPs produced dark MR images as low as 0.04 mg/mL in water and 0.02 mg/mL in cell culture medium. CNA-IONPs evenly distributed in the solution and produced homogenous MR images. The average T2 within the wells of CNA-IONPs in water, PBS and cell culture medium as a function of their concentration were estimated from these images. Plots of relaxation rate (*i.e.* 1/T2) *versus* CNA-IONP concentration showed a linear dependency with correlation coefficients nearly 1 in all three media (data not shown). From the slope of 1/T2 *vs* particle concentration curves, we estimated CNA-IONP relaxivities to be 70, 63 and 73/s/mM Fe in water, PBS and cell culture medium, respectively. Previous research showed that IONPs have T2 relaxivities around 30/s/mM Fe (18,43,64). Contrast efficiency was considerably enhanced by CNA-IONPs compared with Citrate-IONPs. We tried to estimate relaxivities for the T2* relaxation rates (1/T2*, s^{-1}) measurements in a similar way. However, the T2* was so low for the samples that the measurements were not reliable. Nevertheless, the ratio of T2* relaxivity and T2 relaxivity (R2*/R2, $mM^{-1}s^{-1}$) would be high, indicating the potential of the CNA-IONPs to strongly influence the contrast on either T2* or T2 weighted MRI. Previous clinical investigation showed that IONPs with diameters less than 40 nm can accumulate at the margins of human brain tumors resulting in improvement of their delineation on MRI (16). Therefore, CNA-IONPs are expected to significantly

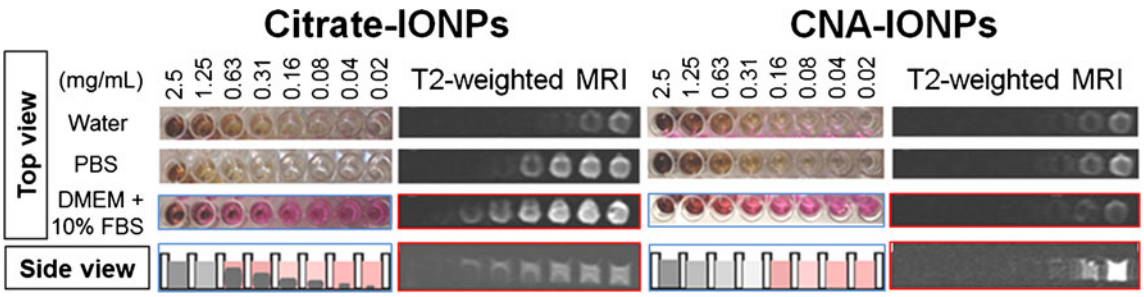

Fig. 7 Visual images and T2-weighted MRI of Citrate-IONPs and CNA-IONPs. Serial dilutions of the samples were prepared on a 96-well plate, containing water, PBS, and DMEM with 10% FBS. Side view images of transverse plane MRIs show dispersion and precipitation of the Citrate-IONPs and lack of CNA-IONP precipitation in DMEM with 10% FBS.

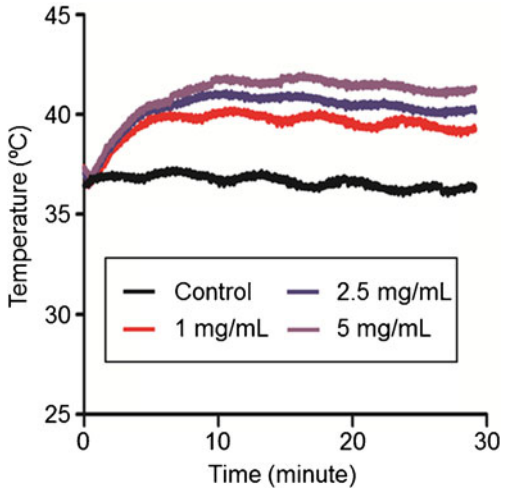

Fig. 8 Heating profiles of CNA-IONPs in the presence of AMF. Three concentrations (1, 2.5, and 5 mg/mL) were tested for fine-tuned remote heating with 30 min applications of AMF. Control indicates the initial temperature of cell culture medium containing no CNA-IONPs (37°C).

improve contrast efficiency and serve as excellent T2 contrast agents in future *in vivo* applications.

AMF-Induced Heating Profiles and Particle Stability After AMF Exposure

Another exciting application of IONPs is AMF-mediated remote heating hyperthermia. CNA-IONPs in cell culture media generated heat in response to AMF, increasing the solution temperature in a concentration-dependent manner (Fig. 8). The solution temperature reached equilibrium in 10 min at 40, 41 and 42°C with 1, 2.5 and 5 mg/mL CNA-IONPs, respectively. This temperature range is promising because previous results demonstrated that cancer cells were susceptible to >40°C and IONP-induced local hyperthermia appeared effective to kill glioma T-9 cells in Fisher F344 rats (7,11). CNA-IONPs in cell culture media exposed to AMF for 30 min were subsequently incubated for 30 h at 37°C, yet the AMF caused no adverse changes in particle sizes of CNA-IONPs (Fig. 5c). Although no large aggregates were formed, the particle sizes of CNA-IONPs increased slightly at 2.5 and 5 mg/mL, following 30 min AMF exposure and subsequent 30 h at 37°C. Such an increase was not shown in 1 mg/mL CNA-IONPs. We found that the particle sizes were consistent for all 1 mg/mL CNA-IONPs incubated at 22, 37, and 43°C for 30 h continuously or after 30 min AMF exposure. These results suggested that the increase in particle sizes of 2.5 and 5 mg/mL CNA-IONPs following 30 min AMF exposure might be attributed not to interparticular aggregates during AMF-induced heat generation but to molecular vibration of IONPs entrapped in CNAs, causing relaxation and rearrangement of block copolymer segments in the CNA core. Despite the slight increase in the particle size, CNA-IONPs were always smaller than 40 nm after 30 h at 37°C in cell culture media regardless of AMF exposure, indicating that IONPs can remain entrapped stably inside CNAs without compromising AMF-responsive magnetic properties. These results suggested that CNA-IONPs would be a promising nanoscale tool to achieve localized hyperthermia *in vivo*, an elegant thermal therapy that invokes little damage to critical organs or tissues such as the central nervous system compared with whole body hyperthermia, which often leads to potential toxicities to the brain (65), or to develop a multifunctional nanoparticle for theranostic applications by delivering IONPs in combination with various therapeutic agents (9,14).

CONCLUSIONS

CNA-IONPs, block copolymer cross-linked nanoassemblies entrapping superparamagnetic Fe_3O_4 iron oxide in a cross-linked core, showed controlled particle size in biological conditions and less toxicity without loss of magnetic properties in comparison to Citrate-IONPs, conventional iron oxide formulations stabilized with citric acid. CNA-IONPs did not agglomerate in water, PBS, or cell culture media, maintaining a clinically-relevant particle size (< 40 nm), suggesting that such stable and small CNA-IONPs may achieve preferential accumulation in tumors and reduced macrophage uptake *in vivo*. Cytotoxicity of CNA-IONPs was significantly lower than that of Citrate-IONPs, causing no cell death up to 10 mg/mL using a murine brain endothelial cell line (bEnd.3). For MRI contrast agent application, CNA-IONPs showed concentration-dependent T2-weighted MRIs with correlation coefficients nearly 1 between CNA-IONP concentrations and T2-weighted MRIs. CNA-IONPs considerably enhanced the T2 relaxivities compared to Citrate-IONPs. CNA-IONPs retained the magnetic properties of IONPs, which generated heat at mild hyperthermic temperatures (40~42°C) in the presence of AMF. In conclusion, CNA-IONPs significantly improved particle stability and biocompatibility of IONPs, and thus provide a promising iron oxide nanoparticle formulation for MRI and AMF-induced remote hyperthermia with low toxicity and high efficiency.

ACKNOWLEDGMENTS AND DISCLOSURES

MD and DS acknowledge the financial support from a NCI-CNTC (National Cancer Institute Cancer Nanotechnology

Training Center) predoctoral and postdoctoral traineeship (NCI 5R25CA153954).

REFERENCES

1. Satarkar NS, Biswal D, Hilt JZ. Hydrogel nanocomposites: a review of applications as remote controlled biomaterials. Soft Matter. 2010;6:2364–71.
2. Frimpong RA, Hilt JZ. Magnetic nanoparticles in biomedicine: synthesis, functionalization and applications. Nanomedicine. 2010;5:1401–14.
3. Hadjipanayis CG, Machaidze R, Kaluzova M, Wang L, Schuette AJ, Chen H, Wu X, Mao H. EGFRvIII antibody-conjugated iron oxide nanoparticles for magnetic resonance imaging-guided convection-enhanced delivery and targeted therapy of glioblastoma. Cancer Res. 2010;70:6303–12.
4. Muldoon LL, Sandor M, Pinkston KE, Neuwelt EA. Imaging, distribution, and toxicity of superparamagnetic iron oxide magnetic resonance nanoparticles in the rat brain and intracerebral tumor. Neurosurgery. 2005;57:785–96.
5. Rock JP, Parsa AT, Rutka JT. Imaging, distribution, and toxicity of superparamagnetic iron oxide magnetic resonance nanoparticles in the rat brain and intracerebral tumor - comments. Neurosurgery. 2005;57:796.
6. Krishnan KM. Biomedical nanomagnetics: a spin through possibilities in imaging, diagnostics, and therapy. IEEE T Magn. 2010;46:2523–58.
7. Silva AC, Oliveira TR, Mamani JB, Malheiros SMF, Malavolta L, Pavon LF, Sibov TT, Amaro E, Tannus A, Vidoto ELG, Martins MJ, Santos RS, Gamarra LF. Application of hyperthermia induced by superparamagnetic iron oxide nanoparticles in glioma treatment. Int J Nanomed. 2011;6:591–603.
8. Stephen ZR, Kievit FM, Zhang M. Magnetite nanoparticles for medical MR imaging. Mater Today. 2011;14:330–8.
9. Weinstein JS, Varallyay CG, Dosa E, Gahramanov S, Hamilton B, Rooney WD, Muldoon LL, Neuwelt EA. Superparamagnetic iron oxide nanoparticles: diagnostic magnetic resonance imaging and potential therapeutic applications in neurooncology and central nervous system inflammatory pathologies, a review. J Cerebr Blood F Met. 2010;30:15–35.
10. Wankhede M, Bouras A, Kaluzova M, Hadjipanayis CG. Magnetic nanoparticles: an emerging technology for malignant brain tumor imaging and therapy. Expert Rev Clin Pharmacol. 2012;5:173–86.
11. Yanase M, Shinkai M, Honda H, Wakabayashi T, Yoshida J, Kobayashi T. Intracellular hyperthermia for cancer using magnetite cationic liposomes: *Ex vivo* study. Jpn J Cancer Res. 1997;88:630–2.
12. Mahmoudi M, Sant S, Wang B, Laurent S, Sen T. Superparamagnetic iron oxide nanoparticles (SPIONs): development, surface modification and applications in chemotherapy. Adv Drug Deliv Rev. 2011;63:24–46.
13. Meenach SA, Anderson KW, Hilt JZ. Synthesis and characterization of thermoresponsive poly(ethylene glycol)-based hydrogels and their magnetic nanocomposites. J Polym Sci Pol Chem. 2010;48:3229–35.
14. Cavaliere R, Ciocatto EC, Giovanella BC, Heidelberger C, Johnson RO, Margottini M, Mondovi B, Moricca G, Rossi-Fanelli A. Selective heat sensitivity of cancer cells. Biochemical and clinical studies. Cancer. 1967;20:1351–81.
15. Maier-Hauff K, Ulrich F, Nestler D, Niehoff H, Wust P, Thiesen B, Orawa H, Budach V, Jordan A. Efficacy and safety of intratumoral thermotherapy using magnetic iron-oxide nanoparticles combined with external beam radiotherapy on patients with recurrent glioblastoma multiforme. J Neuro-Oncol. 2011;103:317–24.
16. Huang HC, Barua S, Sharma G, Dey SK, Rege K. Inorganic nanoparticles for cancer imaging and therapy. J Control Release. 2011;155:344–57.
17. Lin MM, Kim Do K, El Haj AJ, Dobson J. Development of superparamagnetic iron oxide nanoparticles (SPIONS) for translation to clinical applications. IEEE T Nanobiosci. 2008;7:298–305.
18. Gupta AK, Gupta M. Synthesis and surface engineering of iron oxide nanoparticles for biomedical applications. Biomaterials. 2005;26:3995–4021.
19. Farrell D, Majetich SA, Wilcoxon JP. Preparation and characterization of monodisperse Fe nanoparticles. J Phys Chem B. 2003;107:11022–30.
20. Lu AH, Salabas EL, Schuth F. Magnetic nanoparticles: synthesis, protection, functionalization, and application. Angew Chem Int Ed. 2007;46:1222–44.
21. Lodhia J, Mandarano G, Ferris N, Eu P, Cowell S. Development and use of iron oxide nanoparticles (Part 1): Synthesis of iron oxide nanoparticles for MRI. Biomed Imaging Interv J. 2010;6:e12.
22. Novotna B, Jendelova P, Kapcalova M, Rossner P, Turnovcova K, Bagryantseva Y, Babic M, Horak D, Sykova E. Oxidative damage to biological macromolecules in human bone marrow mesenchymal stromal cells labeled with various types of iron oxide nanoparticles. Toxicol Lett. 2012;210:53–63.
23. Mahmoudi M, Hofmann H, Rothen-Rutishauser B, Petri-Fink A. Assessing the *in vitro* and *in vivo* toxicity of superparamagnetic iron oxide nanoparticles. Chem Rev. (2011).
24. Beduneau A, Ma Z, Grotepas CB, Kabanov A, Rabinow BE, Gong N, Mosley RL, Dou H, Boska MD, Gendelman HE. Facilitated monocyte-macrophage uptake and tissue distribution of superparmagnetic iron-oxide nanoparticles. PLoS One. 2009;4:e4343.
25. Kobayashi T. Cancer hyperthermia using magnetic nanoparticles. Biotech J. 2011;6:1342–7.
26. Rumenapp C, Gleich B, Haase A. Magnetic nanoparticles in magnetic resonance imaging and diagnostics. Pharm Res. 2012;29:1165–79.
27. Qiao RR, Yang CH, Gao MY. Superparamagnetic iron oxide nanoparticles: from preparations to *in vivo* MRI applications. J Mater Chem. 2009;19:6274–93.
28. Meenach SA, Hilt JZ, Anderson KW. Poly(ethylene glycol)-based magnetic hydrogel nanocomposites for hyperthermia cancer therapy. Acta Biomater. 2010;6:1039–46.
29. Wagner M, Wagner S, Schnorr J, Schellenberger E, Kivelitz D, Krug L, Dewey M, Laule M, Hamm B, Taupitz M. Coronary MR angiography using citrate-coated very small superparamagnetic iron oxide particles as blood-pool contrast agent: initial experience in humans. J Magn Reson Imaging. 2011;34:816–23.
30. Di Marco M, Sadun C, Port M, Guilbert I, Couvreur P, Dubernet C. Physicochemical characterization of ultrasmall superparamagnetic iron oxide particles (USPIO) for biomedical application as MRI contrast agents. Int J Nanomed. 2007;2:609–22.
31. Chanteau B, Fresnais J, Berret JF. Electrosteric enhanced stability of functional sub-10 nm cerium and iron oxide particles in cell culture medium. Langmuir. 2009;25:9064–70.
32. Goloverda G, Jackson B, Kidd C, Kolesnichenko V. Synthesis of ultrasmall magnetic iron oxide nanoparticles and study of their colloid and surface chemistry. J Magn Magn Mater. 2009;321:1372–6.
33. Park Y, Whitaker RD, Nap RJ, Paulsen JL, Mathiyazhagan V, Doerrer LH, Song YQ, Hurlimann MD, Szleifer I, Wong JY. Stability of superparamagnetic iron oxide nanoparticles at

different pH values: experimental and theoretical analysis. Langmuir. 2012;28:6246–55.
34. Hatakeyama M, Kishi H, Kita Y, Imai K, Nishio K, Karasawa S, Masaike Y, Sakamoto S, Sandhu A, Tanimoto A, Gomi T, Kohda E, Abe M, Handa H. A two-step ligand exchange reaction generates highly water-dispersed magnetic nanoparticles for biomedical applications. J Mater Chem. 2011;21:5959–66.
35. Lattuada M, Hatton TA. Functionalization of monodisperse magnetic nanoparticles. Langmuir. 2007;23:2158–68.
36. Guo R, Song Y, Wang GL, Murray RW. Does core size matter in the kinetics of ligand exchanges of monolayer-protected Au clusters? J Am Chem Soc. 2005;127:2752–7.
37. Woehrle GH, Brown LO, Hutchison JE. Thiol-functionalized, 1.5-nm gold nanoparticles through ligand exchange reactions: scope and mechanism of ligand exchange. J Am Chem Soc. 2005;127:2172–83.
38. Safi M, Courtois J, Seigneuret M, Conjeaud H, Berret JF. The effects of aggregation and protein corona on the cellular internalization of iron oxide nanoparticles. Biomaterials. 2011;32:9353–63.
39. Andreas K, Georgieva R, Ladwig M, Mueller S, Notter M, Sittinger M, Ringe J. Highly efficient magnetic stem cell labeling with citrate-coated superparamagnetic iron oxide nanoparticles for MRI tracking. Biomaterials. (2012).
40. Kumagai M, Imai Y, Nakamura T, Yamasaki Y, Sekino M, Ueno S, Hanaoka K, Kikuchi K, Nagano T, Kaneko E, Shimokado K, Kataoka K. Iron hydroxide nanoparticles coated with poly(ethylene glycol)-poly(aspartic acid) block copolymer as novel magnetic resonance contrast agents for *in vivo* cancer imaging. Colloid Surface B. 2007;56:174–81.
41. Kim DH, Rozhkova EA, Rajh T, Bader SD, Novosad V. Synthesis of hybrid gold/iron oxide nanoparticles in block copolymer micelles for imaging, drug delivery, and magnetic hyperthermia. IEEE T Magn. 2009;45:4821–4.
42. Euliss LE, Grancharov SG, O'Brien S, Deming TJ, Stucky GD, Murray CB, Held GA. Cooperative assembly of magnetic nanoparticles and block copolypeptides in aqueous media. Nano Lett. 2003;3:1489–93.
43. Berret JF, Schonbeck N, Gazeau F, El Kharrat D, Sandre O, Vacher A, Airiau M. Controlled clustering of superparamagnetic nanoparticles using block copolymers: design of new contrast agents for magnetic resonance imaging. J Am Chem Soc. 2006;128:1755–61.
44. Kim BS, Qiu JM, Wang JP, Taton TA. Magnetomicelles: composite nanostructures from magnetic nanoparticles and crosslinked amphiphilic block copolymers. Nano Lett. 2005;5:1987–91.
45. Kim S, Shi YZ, Kim JY, Park K, Cheng JX. Overcoming the barriers in micellar drug delivery: loading efficiency, *in vivo* stability, and micelle-cell interaction. Expert Opin Drug Del. 2010;7:49–62.
46. Lee HJ, Bae Y. Cross-linked nanoassemblies from poly(ethylene glycol)-poly(aspartate) block copolymers as stable supramolecular templates for particulate drug delivery. Biomacromolecules. 2011;12:2686–96.
47. Scott D, Rohr J, Bae Y. Nanoparticulate formulations of mithramycin analogs for enhanced cytotoxicity. Int J Nanomed. 2011;6:2757–67.
48. Ponta A, Akter S, Bae Y. Degradable cross-linked nanoassemblies as drug carriers for heat shock protein 90 inhibitor 17-N-allylamino-17-demethoxygeldanamycin. Pharmaceuticals. 2011;4:1281–92.
49. Frimpong RA, Dou J, Pechan M, Hilt JZ. Enhancing remote controlled heating characteristics in hydrophilic magnetite nanoparticles *via* facile co-precipitation. J Magn Magn Mater. 2010;322:326–31.
50. O'Brien J, Wilson I, Orton T, Pognan F. Investigation of the Alamar blue (resazurin) fluorescent dye for the assessment of mammalian cell cytotoxicity. Eur J Biochem. 2000;267:5421–6.
51. Forrest ML, Yanez JA, Remsberg CM, Ohgami Y, Kwon GS, Davies NM. Paclitaxel prodrugs with sustained release and high solubility in poly(ethylene glycol)-b-poly(epsilon-caprolactone) micelle nanocarriers: pharmacokinetic disposition, tolerability, and cytotoxicity. Pharm Res. 2008;25:194–206.
52. Tantra R, Tompkins J, Quincey P. Characterisation of the de-agglomeration effects of bovine serum albumin on nanoparticles in aqueous suspension. Colloid Surface B. 2010;75:275–81.
53. Allouni ZE, Cimpan MR, Hol PJ, Skodvin T, Gjerdet NR. Agglomeration and sedimentation of TiO2 nanoparticles in cell culture medium. Colloid Surface B. 2009;68:83–7.
54. Foucaud L, Wilson MR, Brown DM, Stone V. Measurement of reactive species production by nanoparticles prepared in biologically relevant media. Toxicol Lett. 2007;174:1–9.
55. Neuberger T, Schöpf B, Hofmann H, Hofmann M, von Rechenberg B. Superparamagnetic nanoparticles for biomedical applications: possibilities and limitations of a new drug delivery system. J Magn Magn Mater. 2005;293:483–96.
56. Varanda LC, Jafelicci M, Tartaj P, O' Grady K, Gonzalez-Carreno T, Morales MP, Munoz T, Serna CJ. Structural and magnetic transformation of monodispersed iron oxide particles in a reducing atmosphere. J Appl Phys. 2002;92:2079–85.
57. Owens DE, Peppas NA. Opsonization, biodistribution, and pharmacokinetics of polymeric nanoparticles. Int J Pharm. 2006;307:93–102.
58. Deng ZJ, Mortimer G, Schiller T, Musumeci A, Martin D, Minchin RF. Differential plasma protein binding to metal oxide nanoparticles. Nanotechnology. 2009;20:455101–9.
59. Li M, Al-Jamal KT, Kostarelos K, Reineke J. Physiologically based pharmacokinetic modeling of nanoparticles. ACS Nano. 2010;4:6303–17.
60. Cole AJ, David AE, Wang J, Galbán CJ, Hill HL, Yang VC. Polyethylene glycol modified, cross-linked starch-coated iron oxide nanoparticles for enhanced magnetic tumor targeting. Biomaterials. 2011;32:2183–93.
61. Khan MI, Mohammad A, Patil G, Naqvi SA, Chauhan LK, Ahmad I. Induction of ROS, mitochondrial damage and autophagy in lung epithelial cancer cells by iron oxide nanoparticles. Biomaterials. 2012;33:1477–88.
62. Berry CC, Wells S, Charles S, Curtis AS. Dextran and albumin derivatised iron oxide nanoparticles: influence on fibroblasts *in vitro*. Biomaterials. 2003;24:4551–7.
63. Soenen SJ, De Cuyper M. Assessing iron oxide nanoparticle toxicity *in vitro*: current status and future prospects. Nanomedicine. 2010;5:1261–75.
64. Hu JM, Qian YF, Wang XF, Liu T, Liu SY. Drug-loaded and superparamagnetic iron oxide nanoparticle surface-embedded amphiphilic block copolymer micelles for integrated chemotherapeutic drug delivery and MR imaging. Langmuir. 2012;28:2073–82.
65. Kiyatkin EA, Sharma HS. Permeability of the blood–brain barrier depends on brain temperature. Neuroscience. 2009;161:926–39.